Analysis of a loaded induction bearingless motor

J. A. Santisteban[1] and R. M. Stephan[2]
[1]CTC/TEE Universidade Federal Fluminense
Rua Passo da Pátria 156, Niterói, RJ, Boa Viagem, Brazil.
[2]EE/COPPE Universidade Federal do Rio de Janeiro
C. P. 68504, Rio de Janeiro, RJ, 21945-970, Brazil.
e-mail: jasl@pcshop.com.br ; richard@coe.ufrj.br

***Abstract* - The analysis of a loaded induction bearingless electric motor is presented. The reviewed electromagnetic model explains some previous reported problems. Other aspects, like the spatial axis coupling owing to electrical and mechanical reasons, are also discussed. A laboratory prototype of this motor was constructed and simulations and experimental results validated this analysis. These new contributions suggest the design of more sofisticated controllers.**

I. INTRODUCTION

Bearingless machine is a broad multidisciplinary field of study. Known approaches rely on the use of additional windings that share the stator volume with the conventional windings used to supply torque [1], [2]. These additional windings make the same function of separated active magnetic bearings.

On the other hand, an alternative approach, which has been proposed on [3], claims the use of the own conventional motor windings (responsible for the torque generation) in order to do also radial positioning. This original approach is favored for operation in the vertical position (that means, the effect of the own weight is minimized). Up to some years ago, experiments were carried out without load and starting problems, were reported [3]. The continuation of this research has established better comprehension of behaviors (electrical and mechanical) not explained before and also the limitations of this approach. Additionally, some strategies of starting and control on loaded conditions are proposed.

II. ELECTROMAGNETIC ANALYSIS

To validate the present approach a laboratory prototype was constructed. It consists of a four poles biphase induction motor, whose "a" phase windings are supplied trough four one phase inverters while a fifth one supplies the windings of phase "b". This motor operates in the vertical position, so the effect of weight is minimized. In order to levitate axially the rotor, an electromagnetic bearing or a superconductor levitator could be used [4]. Meanwhile, in order to simulate this axial bearing, a mechanical bearing in the bottom side was installed. Figure 1 shows the actual distribution of stator windings and figure 2 shows details of the mechanical construction.

Initially, a preliminary analysis without rotor currents will be considered. Later, the complete dynamic problem will be analyzed, that is, considering the presence of the currents in the rotor cage and also the rotation. As it will be shown, both speed and load modify the positioning forces.

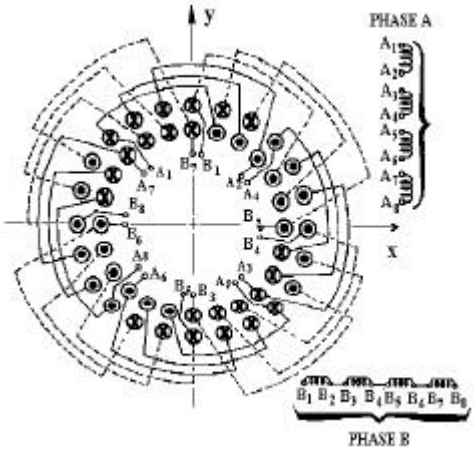

Fig. 1 Set of stator windings of the biphase induction machine.

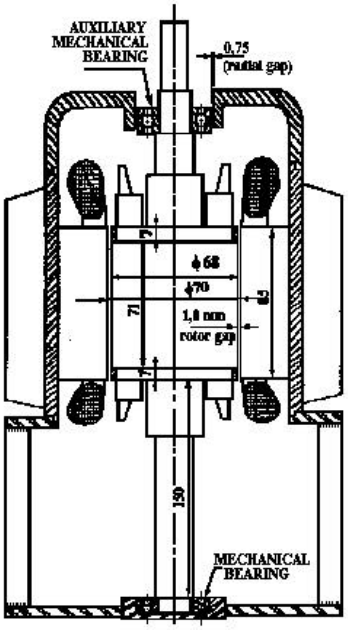

Fig.2 Mechanical structure of the machine.

A. Analysis without rotor currents:

In this item it will be supposed an induction motor without rotor currents. If time continuous currents [i] are imposed in each stator winding, an equivalent magnetic circuit can be solved to obtain their correspondents (with some simplifications) equivalent polar airgap linkage fluxes. The equivalent magnetic scheme for phase "a" is shown in Fig. 3 and its corresponding magnetic circuit in Fig. 4.

The linked fluxes [l] are related to the currents [i] as given by Eq. (1). The magnetic circuit equations are given in Eq. (2). The net force (F_e) along an axis can be calculated taking the derivative of the total magnetic energy inside the airgap (W_e) with respect to the displacement (h).

$$[\,l\,] = [L(h)][i] \tag{1}$$

$$\begin{bmatrix} l_{y1} \\ l_{y2} \\ l_{x1} \\ l_{x2} \end{bmatrix} = N^2 \begin{bmatrix} \frac{1}{R_{y1}} - \frac{R_{eq}}{R_{y1}^2} & -\frac{R_{eq}}{R_{y1}R_{y2}} & -\frac{R_{eq}}{R_{y1}R_{x1}} & -\frac{R_{eq}}{R_{y1}R_{x2}} \\ -\frac{R_{eq}}{R_{y2}R_{y1}} & \frac{1}{R_{y2}} - \frac{R_{eq}}{R_{y2}^2} & -\frac{R_{eq}}{R_{y2}R_{x1}} & -\frac{R_{eq}}{R_{y2}R_{x2}} \\ -\frac{R_{eq}}{R_{x1}R_{y1}} & -\frac{R_{eq}}{R_{x1}R_{y2}} & \frac{1}{R_{x1}} - \frac{R_{eq}}{R_{x1}} & -\frac{R_{eq}}{R_{x1}R_{x2}} \\ -\frac{R_{eq}}{R_{x2}R_{y1}} & -\frac{R_{eq}}{R_{x2}R_{y2}} & -\frac{R_{eq}}{R_{x2}R_{x1}} & \frac{1}{R_{x2}} - \frac{R_{eq}}{R_{x2}^2} \end{bmatrix} \begin{bmatrix} i_{y1} \\ i_{y2} \\ i_{x1} \\ i_{x2} \end{bmatrix} \tag{2}$$

$$W_e = \frac{1}{2}[i]^{\mathrm{T}}[L(h)][i] \tag{3}$$

$$F_e = \frac{dW_e}{dh} \tag{4}$$

$$F_e = \frac{1}{2}[i]^{\mathrm{T}} \frac{d[L(h)]}{dh}[i]. \tag{5}$$

Where $L(h)$ is the inductance matrix whose components are a function of the radial rotor displacements. Each reluctance (R) is calculated as: $R = m\frac{h}{A}$, with "A" being the mean area of each magnetic pole, "h" the correspondent airgap (x1, x2, y1 or y2) and $\frac{1}{R_{eq}} = \frac{1}{R_{y1}} + \frac{1}{R_{y2}} + \frac{1}{R_{x1}} + \frac{1}{R_{x2}}$.

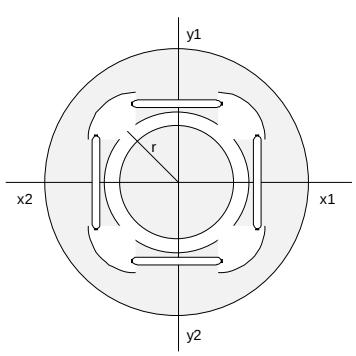

Fig. 3. Equivalent magnetic scheme.

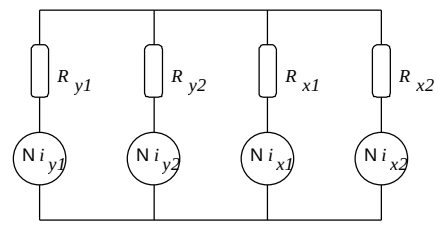

Fig. 4. Equivalent magnetic circuit.

With the new variables "x" and "y" such that: $y1 = y = h_o + \Delta y$; $y2 = (2 * h_o - y) = h_o - \Delta y$; $x1 = x = h_o + \Delta x$ and $x2 = (2 * h_o - x) = h_o - \Delta x$, where h_o is the nominal airgap in the centered condition, the first term of the inductance matrix $L_{11}(h)$ will be:

$$L_{11} = m\,AN^2 \left[\frac{1}{y} - \frac{1}{2h_o\left(\frac{y^2}{x(2h_o - x)} + \frac{y}{(2h_o - y)} \right)} \right]. \tag{6}$$

Analogously, with some simplifications, the other terms can be calculated and then the derivative of [$L(h)$] with respect to the displacement y will be:

$$\frac{\P[L(h)]}{\P y} = -\frac{1}{2} N^2 m \frac{A}{y^2} \begin{bmatrix} 1 & 0 & -\frac{1}{2} & -\frac{1}{2} \\ 0 & -1 & +\frac{1}{2} & +\frac{1}{2} \\ -\frac{1}{2} & +\frac{1}{2} & 0 & 0 \\ -\frac{1}{2} & +\frac{1}{2} & 0 & 0 \end{bmatrix}. \tag{7}$$

Then, using Eq. (5), the equivalent net force along y will be:

$$F_y = -\frac{1}{4} \mathrm{N}^2 m \frac{A}{y^2} \left[i_{y1}^2 - i_{y2}^2 - i_{y1}(i_{x1} + i_{x2}) + i_{y2}(i_{x1} + i_{x2}) \right]. \tag{8}$$

It should be noted that the radial force depends on all the winding currents. On the other hand, the positioning strategy is based on the modulation of the current amplitude in such a way that while a reference current for a winding is incremented, the reference current for the opposed winding is decreased in the same magnitude. Thus, the instantaneous currents imposed in phase "a" will be:

$$i_{y1} = (i_o + \Delta i_y)\cos w\,t, \tag{9}$$

$$i_{y2} = (i_o - \Delta i_y)\cos w\,t, \tag{10}$$

$$i_{x1} = -(i_o + \Delta i_x)\cos w\,t, \tag{11}$$

$$i_{x2} = -(i_o - \Delta i_x)\cos w\,t, \tag{12}$$

where i_o is a mean current value which will determine an average stiffness for the bearing behavior of the motor, and Δi is the incremental value supplied by the position control. Thus, the net force along the "y" axis may be expressed as:

$$F_y = -2\,\mathrm{N}^2 m \frac{A}{y^2}\left[i_o\,\Delta i_y\right]\cos^2 wt\,. \qquad (13)$$

As $\cos^2 \omega t = (1/2)[1+\cos 2\,\omega t]$ this force can be split in two terms: a continuous force and a harmonic component. As long as the natural frequencies of the rotor are kept reasonably lower than this harmonic value, the oscillatory term should produce a negligible effect on the dynamic behavior of the system. This force is non linear, but for small displacements ($\Delta y < y$) depends basically on Δi_y.

When coils are excited with continuous currents, equation (13) can be even used doing $\cos^2 \omega t$ equal to the unit. In both cases, the net radial force is proportional to the differential current Δi_y.

From the mechanical specifications, one can find the following dimensions: y=1e-3 m., A= 3.734e-3m^2, N= 50 equivalent coils and the height of the rotor l= 85e-3 m. With i_o=1.5A, equation (13) can be plotted as shown in figure 5.

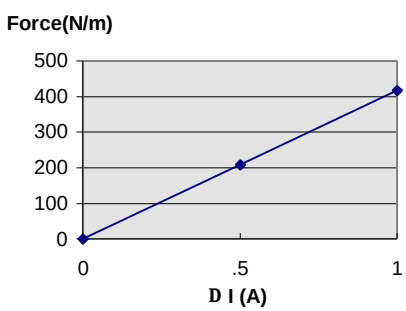

Fig. 5 Analytical magnetic positioning force.

This analytical approach is very close to simulation results using the finite elements program ANSYS 5.3 [5], [9].

B. Analysis with rotor currents:

It is known that for a generic electromagnetic system, the magnetic energy (W_f) stored in it (airgap), is described by the following equation [6]:

$$W_f = \int i d\,l\,.$$

And, in the case of J supply sources:

$$W_f = \int \sum_{j=1}^{J} i d\,l$$

Additionally, if the system is considered magnetically linear:

$$W_f = \frac{1}{2}[i_1\, i_2 \ldots i_n]\begin{bmatrix} L_{11}(h) & L_{12}(h) & \ldots & \ldots \\ L_{21}(h) & L_{22}(h) & \ldots & \ldots \\ \ldots & \ldots & \ldots & \ldots \\ \ldots & \ldots & \ldots & L_{nn}(h) \end{bmatrix}\begin{bmatrix} i_1 \\ i_2 \\ \ldots \\ i_n \end{bmatrix} \qquad (14)$$

In the present case, the total current vector [i] is given not only by all the stator currents but also by the modeled rotor currents.

$$[i] = [i_{sA} i_{sB}\, i_{ra}\, i_{rb}]^T$$
$$[i_{sA}] = [i_{y1}\, i_{y2}\, i_{x1}\, i_{x2}]^T$$
$$[i_{sB}] = [i_{y'1}\, i_{y'2}\, i_{x'1}\, i_{x'2}]^T$$
$$[i_{ra}] = [i_{l1}\, i_{l2}\, i_{m1}\, i_{m2}]^T$$
$$[i_{rb}] = [i_{l'1}\, i_{l'2}\, i_{m'1}\, i_{m'2}]^T$$

On the other hand, the inductance matrix has the following form:

$$\begin{bmatrix} L_{sAsA} & L_{sAsB} & L_{sAra} & L_{sArb} \\ L_{sBsA} & L_{sBsB} & L_{sBra} & L_{sBrb} \\ L_{rasA} & L_{rasB} & L_{rara} & L_{rarb} \\ L_{rbsA} & L_{rbsB} & L_{rbra} & L_{rbrb} \end{bmatrix},$$

where [L_{sAsA}] was just given in equation (2), and [L_{sAsB}] and [L_{rarb}] are considered nulls [6]. The stator-rotor mutual inductances will depend on the relative position between them. Now, taking the first derivative of equation (14) with respect to h, the net force along the direction h will be:

$$F_e = \frac{1}{2}\left[\left[i_{sA}\right]^T \frac{\P\left[\, l_{sAA}\right]}{\P h} + \left[i_{sB}\right]^T \frac{\P\left[\, l_{sBB}\right]}{\P h} + \right.$$
$$\left. + \left[i_{ra}\right]^T \frac{\P\left[\, l_{raa}\right]}{\P h} + \left[i_{rb}^T\right]^T \frac{\P\left[\, l_{rbb}\right]}{\P h}\right], \qquad (15)$$

where the following terms represent linkage fluxes:

$$l_{sAA} = L_{sAsA}\, i_{sA} + L_{sAra}\, i_{ra} + L_{sArb}\, i_{rb}\,, \qquad (16)$$
$$l_{sBB} = L_{sBsB}\, i_{sB} + L_{sBra}\, i_{ra} + L_{sBrb}\, i_{rb}\,, \qquad (17)$$
$$l_{raa} = L_{rasA}\, i_{sA} + L_{rasB}\, i_{sB} + L_{rara}\, i_{ra}\,, \qquad (18)$$
$$l_{rbb} = L_{rbsA}\, i_{sA} + L_{rbsB}\, i_{sB} + L_{rbrb}\, i_{rb}\,. \qquad (19)$$

As it is seen, rotor currents affect each of these linkage fluxes. In a compact form, the net radial force can be also written as:

$$F_e = \frac{1}{2}\left[\left[i_{sAB}\right]^T \frac{\P\left[\, l_{sAB}\right]}{\P h} + \left[i_{rab}\right]^T \frac{\P\left[\, l_{rab}\right]}{\P h}\right], \qquad (20)$$

On the other hand, because the energy stored in the leakage inductances is not a part of the energy stored in the coupling field, the leakage linkage flux terms should be subtracted from eq. 20. So the following substitutions could be done:

$$\left[\, l_{sAB}\right] \Rightarrow \left[\, l_{sAB}\right] - \left[L_{ls}\right]\left[i_{sAB}\right],$$
$$\left[\, l_{rab}\right] \Rightarrow \left[\, l_{rab}\right] - \left[L_{lr}\right]\left[i_{rab}\right].$$

Where [Lls] e [Llr] are the leakage inductances.

The contribution of rotor currents can also be foreseen observing the conventional steady state model of an induction motor (fig. 6). Imposing a fixed value of stator currents, a rotor current increment will decrease the airgap linkage flux, so, radial forces will also decrease. This happens in the starting as well as in loaded conditions.

This is one of the reasons that explains the former starting problems [3] and also supports the special care on the conception of the position algorithm.

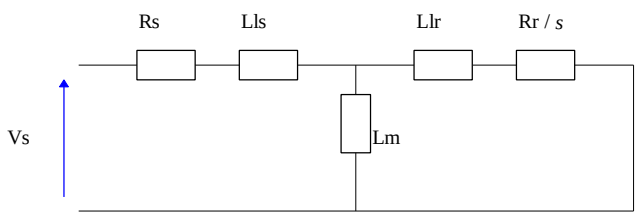

Figure 6.- Steady state induction motor model.

C. Spatial phenomenon :

One implication with respect to the previous item is that the mean airgap flux should be monitored (or estimated) in order to make the adequate adjustment in the position controller, however, there is another important point: when both phases of the motor are supplied with currents, unlike the case when only one phase is supplied, airgap flux is rotating, so, radial force is actually an instantaneous effect inside the motor.

In order to explain this fact and in view of that position sensors are located fixed to the stator, it is of particular interest the electric model on the stationary reference frame. The equations given by the conventional theory of induction machines [6] relate input currents with linkage fluxes and speed. These are validate both in steady state as in transient state (starting or step loading). In figure 7, this model is depicted.

In this figure, the power supplies at the right side of this model depend on the product of speed and the orthogonal component of the rotor flux. From this, it is clear the coupling between the orthogonal components of the airgap flux.

Supposing rotor currents and an instantaneous increment in the i_{ds} current component, there will be variations both on the "d" as in the "q" components of the airgap flux (responsible for the radial positioning). That means that the expected net radial force will not be aligned with the "d" axis as would be expected, so, a correction will be necessary. This correction will depend on the load and the speed.

In figure 8 the effect in a two poles configuration is illustrated. In (a) the phase "a" current and airgap linkage flux components are depicted as a function of the time. In (b), the spatial trajetory of the spatial vector current and airgap linkage flux are shown. Time instants (t1, t2 and t3) are indicated for better comprehension.

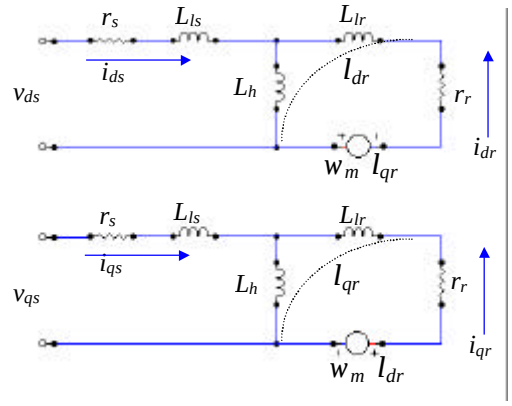

Fig 7. Instantaneous dq model for an induction motor in the stationary reference frame.

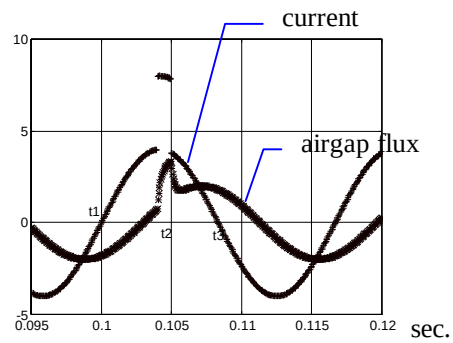

(a) Time components of phase "a".
Current (A) and airgap flux (10^{-1} Weber)

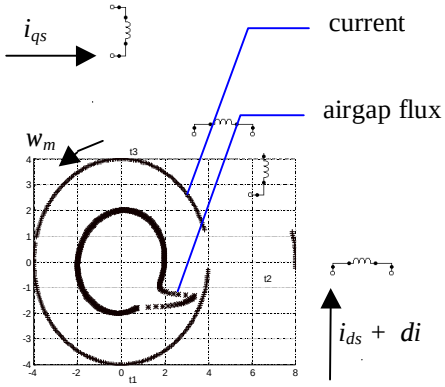

(b) Spatial trajetory

Fig 8. Current and airgap linkage flux after a step increment on current. Two poles case.

As seen, although the effects in the time are simultaneous there is an spatial angular difference.

At steady state, the necessity to correct the angular position of the displacement sensors as load changes is experimentally observed. This change can be made until minimum radial vibrations are obtained. As higher the load, higher also is the angular correction.

Actually, this phenomenon is related to the natural phase difference between the stator currents and the airgap flux. Without load, airgap flux is in phase with stator current, but with load a non zero phase angle appears. In the experimental prototype, the angle correction of the position sensors is made through software.

In order to illustrate the instantaneous spatial behavior of the airgap flux, a current pulse perturbation is added to a phase of the motor while the other phase is unchanged. Three cases were simulated. In figure 9 the motor is starting; in figure 10 the motor is rotating at steady state without load; and in figure 11 the motor is rotating at steady state but loaded. In all cases the imposed currents have 4A in amplitude and 60 Hz frequency. Stator current is identified by the symbol (+) and airgap flux by the symbol (*).

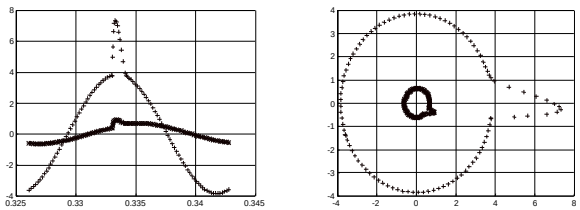

a) b)

Fig. 9.- Response to a current pulse perturbation while starting.
a) Phase "a" current (A) component and airgap flux (10^{-1} Weber) components while starting.
b) Spatial trajectory of stator current(+) and airgap flux(*) vectors.

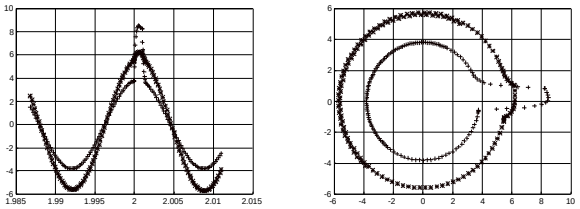

a) b)

Fig. 10.- Response to a current pulse perturbation in steady state without load.
a) Phase "a" current (A) component and airgap flux (10^{-1} Weber) component.
b) Spatial trajectory of stator current(+) and airgap flux(*) vectors.

As shown, in starting conditions the airgap flux amplitude is lower than in steady state and it can also be noted that the spatial airgap flux vector is not in phase with the stator current vector. On the other hand, comparing figures 10 b) and 11 b) the spatial influence of load on the spatial angle of airgap flux can be noted.

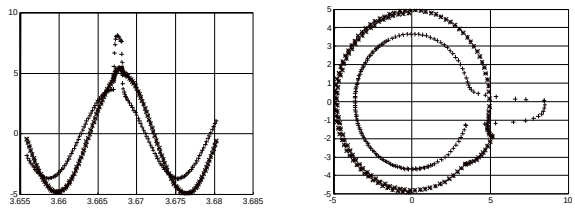

a) b)

Fig. 11.- Response to a current pulse perturbation in steady state with load.
a) Phase "a" current (A) component and airgap flux (10^{-1} Weber) component.
b) Spatial trajectory of stator current(+) and airgap flux(*) vectors.

It should be also pointed out that this angle varies with the supply frequency. In order to illustrate this fact, the variations of airgap current amplitude (a) and its phase (b), with respect to the model in figure 6, are shown in figure 12 for different values of supply frequency. In this case, the unloaded steady state current is imposed to the unloaded motor. Although here it is supposed that motor parameters remain constant along all frequencies, an accurate model will possible indicate even stronger influences. Nevertheless, accurate positioning control should take care of this behavior.

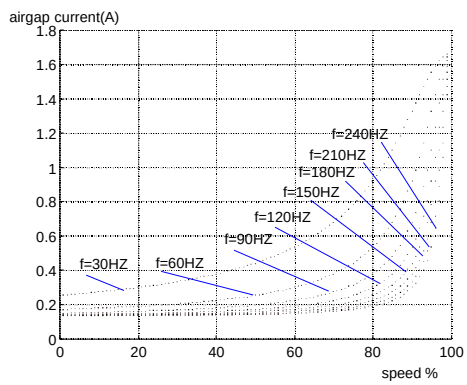

a)

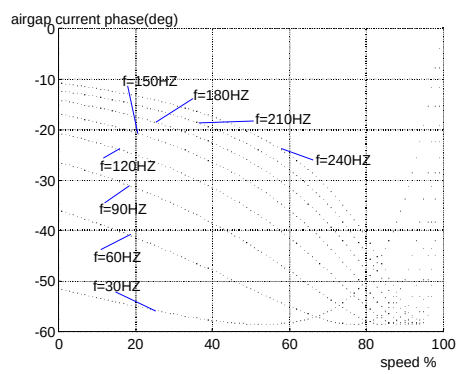

b)

Figure 12.- a) airgap current amplitude vs speed.
b) airgap current phase vs speed.

III. EXPERIMENTAL RESULTS.

In order to probe the previous analysis, a digital control was implemented using the prototype motor shown in figure 2 and a personal computer (133 MHz Pentium). Two PD (Proportional Derivative) positioning controllers were designed based on the mechanical model for low speed [7]. Figure 13 shows the maximum signal trace furnished by the position sensors (0.25mm/div). In figure 14 the position sensors trajectory without(a) and with(b) angle correction is compared, while the motor is unloaded and rotating at 1800 rpm. In this case, the correction angle was 9 degree. Ideally this angle should be null, but because the bottom mechanical bearing it is expected a little load torque.

In figure 15 the behavior of the rotor trajectory with the motor loaded is compared. In this case, the correction angle was 15 degree. The rotor load was implemented using an electromagnetic brake, which furnish not only torque but also radial force.

The circular shape of the trajectories are mainly due to mechanical unbalances.

IV. CONCLUSIONS.

A new electromagnetic model for a previously designed bearingless motor has been described and gives a .better comprehension of the system.

This more accurate model will allow:

- The realization of numerical simulation of the dynamical behavior of the prototype with and without load.
- The design of more sophisticated controllers (e.g., multivariable, robust, fuzzy), taking into account the variables coupling.

Experimental and simulation results validate this approach.

V. REFERENCES

[1] J. Bichsel, "The Bearingless Electrical Machine", *NASA Conference Publication* 3152, part2, 1991.

[2] Chiba, A., Power, D.T., Rahman, M.A.,"Characteristics of a bearingless induction motor", IEEE Trans. Magn., v.27, 1991, pp 5199-5201.

[3] Salazar, A.O., Stephan, R.M., "A bearingless method for induction machines", *IEEE Trans. on Magnetics*, Nov, Vol. 29, No. 6, 1993, pp 2965-2967.

[4] D. David, A. Santisteban, R. Stephan, Y. Gorelov, R. Andrade Jr. A. Pereira, R. Nicolsky, "Passive superconducting axial bearing for an induction motor", *43rd Conference on Magnetism and Magnetic Materials*, paper BP04, Flórida, USA, 9-12 Nov., 1998.

[5] Bessa M. F., Noronha R. F., "Cálculo De Forças Em Mancais Magnéticos - Comparação De Resultados", COBEM 97, Bauru, SP, Dez., 1997.

[6] Krause P. C. et al, *Analysis of Electric Machinery*, IEEE Press, 1995.

[7] Santisteban J.A., Ripper, Stephan R.M., David D., Noronha R., "Controller design for a bearingless electric motor", *Revista Brasileira de Ciências Mecânicas*, Vol. XXI, No. 1, Mar. 1999, pp. 91-98.

[8] Schweitzer G., Bleuler H. and Traxler A., *Active Magnetic Bearings*, v/d|f, 1994.

[9] Ansys ED 5.3, 1997

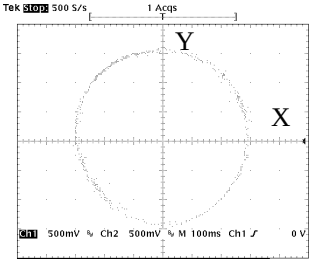

Fig. 13.- Maximum trajectory of rotor measured by the displacement sensors.

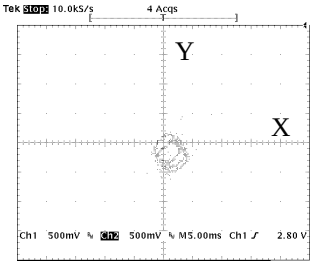

a)

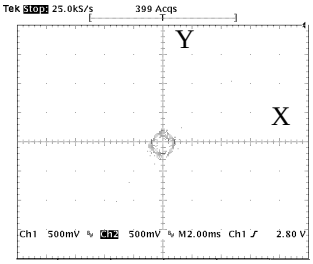

b)

Fig. 14.- Unloaded test: a) without sensor angle correction. b) with sensor angle correction.

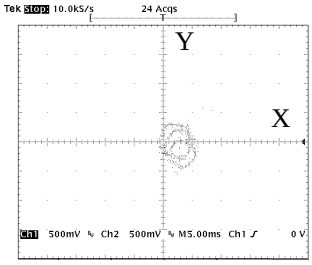

a)

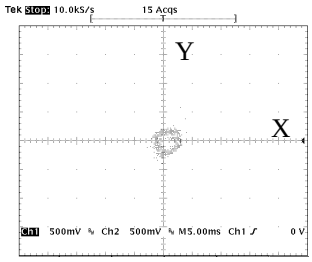

b)

Fig. 15.- Loaded test: a) without sensor angle correction. b) with sensor angle correction.